FERMILAB-Pub-03/327 October 2003

Polarized proton collider at RHIC☆

I. Alekseev[a], C. Allgower[b], M. Bai[c], Y. Batygin[d], L. Bozano[e], K. Brown[c], G. Bunce[c], P. Cameron[c], E. Courant[c], S. Erin[f], J. Escallier[c], W. Fischer[c], R. Gupta[c], K. Hatanaka[g], H. Huang[c], K. Imai[h], M. Ishihara[d], A. Jain[c], A. Lehrach[j], V. Kanavets[a], T. Katayama[i], T. Kawaguchi[d], E. Kelly[c], K. Kurita[c], S.Y. Lee[k], A. Luccio[c], W.W. MacKay[c,*], G. Mahler[c], Y. Makdisi[c], F. Mariam[c], W. McGahern[c], G. Morgan[c], J. Muratore[c], M. Okamura[d], S. Peggs[c], F. Pilat[c], V. Ptitsin[m], L. Ratner[c], T. Roser[c], N. Saito[c], H. Satoh[l], Y. Shatunov[m], H. Spinka[b], M. Syphers[n], S. Tepikian[c], T. Tominaka[d], N. Tsoupas[c], D. Underwood[b], A. Vasiliev[f], P. Wanderer[c], E. Willen[c], H. Wu[d], A. Yokosawa[b], A.N. Zelenski[c]

[a] *ITEP B. Cheremushkinskaja, 25, Moscow 117259, Russia*
[b] *Argonne National Laboratory, 9700 S. Cass Ave., Argonne, IL 60539, USA*
[c] *Brookhaven National Laboratory, Upton, NY 11973-5000, USA*
[d] *RIKEN, Wako-shi, Saitama 351-01, Japan*
[e] *IBM Almaden Res. Ctr., 650 Harry Rd., San Jose, CA 95120, USA*
[f] *IHEP, Protvino, Russia*
[g] *Research Center for Nuclear Physics, Osaka University, Osaka 567-0047, Japan*
[h] *Kyoto University, Sakyo-ku, Kyoto, Japan*
[i] *Center for Nuclear Study, Univ. of Tokyo, Tokyo, Japan*
[j] *Forschungzentrum Jülich Institute für Kernphysik, Jülich, Germany*
[k] *IUCF, University of Indiana, Bloomington, IN, USA*
[l] *KEK, Tsukuba, Ibaraki 305-0801, Japan*
[m] *BINP, Acad. Lavrentiev prospect 11, 630090 Novosibirsk, Russia*
[n] *Fermilab, Box 500, Batavia, IL 60510-0500, USA*

Abstract

In addition to heavy ion collisions (RHIC Design Manual, Brookhaven National Laboratory), RHIC will also collide intense beams of polarized protons (I. Alekseev, et al., Design Manual Polarized Proton Collider at RHIC, Brookhaven National Laboratory, 1998 [2]), reaching transverse energies where the protons scatter as beams of polarized quarks and gluons. The study of high energy polarized protons beams has been a long term part of the program at BNL with the development of polarized beams in the Booster and AGS rings for fixed target experiments. We have extended this

☆Work was performed under the auspices of the U.S. Department of Energy and was supported by grants from the U.S. National Science Foundation and funds from The Institute for Chemical and Physical Research (RIKEN), Japan.
*Corresponding author. Tel.: +1-631-344-3076; fax: +1-631-344-5954.
E-mail addresses: mackay@bnl.gov, waldo@bnl.gov (W.W. MacKay).
URL: http://www.rhichome.bnl.gov/People/waldo.

capability to the RHIC machine. In this paper we describe the design and methods for achieving collisions of both longitudinal and transverse polarized protons in RHIC at energies up to $\sqrt{s} = 500$ GeV.

PACS: 29.20.Dh; 29.25.Lg; 29.20.Lq; 29.27.–a; 29.27.Ac; 29.27.Bd; 29.27.Eg; 29.27.Fh; 29.27.Hj; 41.75.–i; 41.75.Ak; 85.25.Ly

Keywords: RHIC; Polarized protons; Accelerator; Collider; Synchrotron; Storage ring; Siberian snake; Spin rotator; Helical dipole magnet; Beam transport; Polarimetry

1. Introduction

1.1. Spin dynamics and siberian snakes

To achieve high energy polarized proton collisions polarized beams first have to be accelerated which requires an understanding of the evolution of spin during acceleration and the tools to control it. The evolution of the spin direction of a beam of polarized protons in external magnetic fields such as exist in a circular accelerator is governed by the Thomas-BMT equation [2],

$$\frac{d\vec{P}}{dt} = -\left(\frac{e}{\gamma m}\right)[G\gamma\vec{B}_\perp + (1+G)\vec{B}_\parallel] \times \vec{P}, \qquad (1)$$

where the polarization vector $\vec{P}$ is expressed in the frame that moves with the particle. This simple precession equation is very similar to the Lorentz force equation which governs the evolution of the orbital motion in an external magnetic field:

$$\frac{d\vec{v}}{dt} = -\left(\frac{e}{\gamma m}\right)[\vec{B}_\perp] \times \vec{v}. \qquad (2)$$

From comparing these two equations it can readily be seen that, in a pure vertical field, the spin rotates $G\gamma$ times faster than the orbital motion. Here $G = 1.7928$ is the anomalous magnetic moment of the proton and $\gamma = E/m$. In this case the factor $G\gamma$ then gives the number of full spin precessions for every full revolution, a number which is also called the spin tune ν_{sp}. At top RHIC energy (250 GeV) this number reaches 478. The Thomas-BMT equation also shows that at low energies ($\gamma \approx 1$) longitudinal fields $\vec{B}_\parallel$ can be quite effective in manipulating the spin motion, but at high energies transverse fields $\vec{B}_\perp$ need to be used to have any effect beyond the always present vertical holding field.

The acceleration of polarized beams in circular accelerators is complicated by the presence of numerous depolarizing resonances. During acceleration, a depolarizing resonance is crossed whenever the spin precession frequency equals the frequency with which spin-perturbing magnetic fields are encountered. There are two main types of depolarizing resonances corresponding to the possible sources of such fields: *imperfection resonances*, which are driven by magnet errors and misalignments, and *intrinsic resonances*, driven by the focusing fields.

The resonance conditions are usually expressed in terms of the spin tune ν_{sp}. For an ideal planar accelerator, where orbiting particles experience only the vertical guide field, the spin tune is equal to $G\gamma$, as stated earlier. The resonance condition for imperfection depolarizing resonances arises when $\nu_{sp} = G\gamma = n$, where n is an integer. Imperfection resonances are therefore separated by only 523 MeV energy steps. The condition for intrinsic resonances is $\nu_{sp} = G\gamma = kP \pm \nu_y$, where k is an integer, ν_y is the vertical betatron tune and P is the superperiodicity. For example at the Brookhaven AGS, $P = 12$ and $\nu_y \approx 8.8$. For most of the time during the acceleration cycle, the precession axis, or stable spin direction, coincides with the main vertical magnetic field. Close to a resoance, the stable spin direction is perturbed away from the vertical direction by the resonance driving fields. When a polarized beam is accelerated through an isolated resonance, the final polarization can be calculated analytically [3] and is given by

$$P_f/P_i = 2e^{-\frac{\pi|\varepsilon|^2}{2\alpha}} - 1 \qquad (3)$$

where P_i and P_f are the polarizations before and after the resonance crossing, respectively, ε is the

resonance strength obtained from the spin rotation of the driving fields, and α is the change of the spin tune per radian of the orbit angle. When the beam is slowly ($\alpha \ll |\varepsilon|^2$) accelerated through the resonance, the spin vector will adiabatically follow the stable spin direction resulting in spin flip. However, for a faster acceleration rate partial depolarization or partial spin flip will occur. Traditionally, the intrinsic resonances are overcome by using a betatron tune jump, which effectively makes α large, and the imperfection resonances are overcome with the harmonic corrections of the vertical orbit to reduce the resonance strength ε [4]. At high energy, these traditional methods become difficult and tedious.

By introducing a 'Siberian Snake' [5], which generates a 180° spin rotation about a horizontal axis, the stable spin direction remains unperturbed at all times as long as the spin rotation from the Siberian Snake is much larger than the spin rotation due to the resonance driving fields. Therefore the beam polarization is preserved during acceleration. An alternative way to describe the effect of the Siberian Snake comes from the observation that the spin tune with the Snake is a half-integer and energy independent. Therefore, neither imperfection nor intrinsic resonance conditions can ever be met as long as the betatron tune is different from a half-integer.

Such a spin rotator is traditionally constructed by using either solenoidal magnets or a sequence of interleaved horizontal and vertical dipole magnets producing only a local orbit distortion. Since the orbit distortion is inversely proportional to the momentum of the particle, such a dipole snake is particularly effective for high-energy accelerators, e.g. energies above about 30 GeV. For lower-energy synchrotrons, such as the Brookhaven AGS with weaker depolarizing resonances, a partial snake [6], which rotates the spin by less than 180°, is sufficient to keep the stable spin direction unperturbed at the imperfection resonances.

1.2. Polarized proton acceleration at RHIC

By using Siberian Snakes the stage is set for the acceleration of polarized proton beams to much higher energies. Polarized protons from the AGS are injected into the two RHIC rings to allow collisions at center of mass energies up to 500 GeV with both beams polarized. Fig. 1 shows the

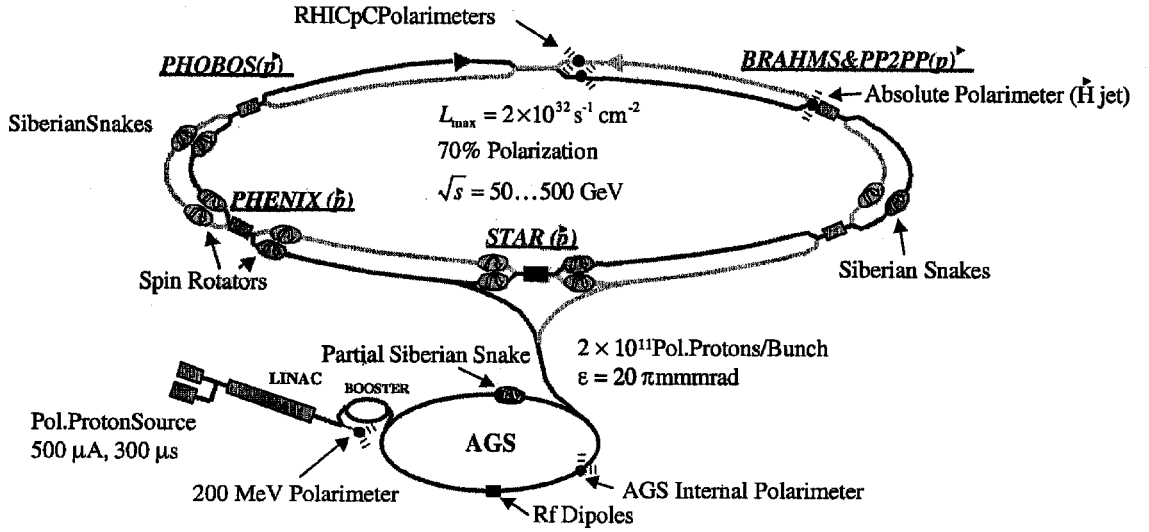

Fig. 1. The Brookhaven hadron facility complex, which includes the AGS Booster, the AGS, and RHIC. The RHIC spin project will install two snakes per ring with four spin rotators per detector for achieving helicity-spin experiments.

layout of the Brookhaven accelerator complex highlighting the components required for polarized beam acceleration.

To maintain polarization during the acceleration process, two full Siberian Snakes are inserted on opposite sides of the RHIC lattice for each of the two counter-rotating rings. In addition to these Snakes, spin rotators are located on each side of the two major interaction points which allow the spin orientation to be altered from the vertical plane to the longitudinal plane. These devices are the primary magnetic components of the polarized beam project at RHIC. In addition, "spin flip" devices will be inserted to allow for the manipulation of the spin orientation during a store, as well as polarimetry instrumentation.

The major elements required for this project are the superconducting magnets for the Siberian Snakes and the Spin Rotators. Each Siberian Snake consists of a set of four superconducting helical dipole magnets. The magnets are capable of producing a central field of up to 4 T which spirals through 360° over a length of approximately 2.4 m. Four such magnets, powered in pairs, can generate a spin rotation from vertically up (the nominal stable spin direction for the synchrotron) to vertically down, with no net excursions of the particle trajectory. This is the function of the Snake. The Spin Rotator is similarly constructed; by altering the "handedness" of two of the helical magnets, and using slightly different fields, the spin can be made to rotate from the vertical to the longitudinal direction.

With one or two Snakes all depolarizing resonances should be avoided since the spin tune is a half-integer independent of energy. However, if the spin disturbance from small horizontal fields is adding up sufficiently between the Snakes, depolarization can still occur. This is most pronounced when the spin rotations from all the focusing fields add up coherently which is the case at the strongest intrinsic resonances. At RHIC two Snakes can still cope with the strongest intrinsic resonance.

To provide RHIC with the capability of polarized beams, a total of 4 Snakes and 8 Rotators are required. Thus, 48 individual full-helical dipole magnets are required. The four magnets needed to create one Snake or one Rotator are mounted inside of a modified RHIC Dipole Magnet cryostat. Since it is desirable to power independently the four magnets within the cryostat, the required current should be minimized in order to keep the heat leak due to the power leads as small as possible. Thus, hundreds of turns are required. The field strengths of the Snake magnets are held constant during the acceleration process, while the appropriate fields in the Rotator magnets are beam energy dependent, and are only powered during beam storage. Design and construction of the snakes and rotators is discussed in Refs. [7,8].

During the course of a polarized colliding beams experiment, it is desirable to reverse adiabatically the direction of the spin to eliminate the possibility of systematic errors. By introducing an oscillating field on resonance with the natural spin precession frequency, such a "spin flip" can occur. A discussion of the hardware used to perform this task is described in Section 5.3. In addition to their use for the experiments, the spin flip devices can be used to measure accurately the spin precession frequency (or, "spin tune") and so will be used during commissioning of the Snakes.

Another major component is the instrumentation used to measure the beam polarization. Polarimetry has two functions: relative and absolute polarization measurements. Relative measurements may use a spin-sensitive process which has a high rate, but is uncalibrated. The two polarimeters (one per ring) use proton–carbon elastic scattering in the Coulomb–nuclear interference (CNI) region to measure the relative polarization. In the future we will install an intense polarized proton jet target. The absolute polarization of the jet would be known, allowing calibration of the CNI proton–carbon polarimeters with the jet. Our goal is absolute polarization to $\Delta P/P = \pm 5\%$. Details of the polarimeter system can be found in Section 6.

2. Polarized proton injector

To meet the required bunch intensity of 2×10^{11} protons per bunch in RHIC, the AGS as the

polarized proton injector will need to reach a bunch intensity of about 4×10^{11} to allow for some losses during the transfer to RHIC for acceleration. Although it would be possible to use the old polarized proton source [9] by accumulating up to twenty source pulses in the Booster, a new optically pumped polarized ion source (OPPIS) has been installed. The new polarized H^- source produces 500 μA in a single 300 μs pulse, which corresponds to 9×10^{11} polarized H^-. This is sufficient intensity to eliminate the need for the accumulation in the Booster. The polarized H^- ions are accelerated to 200 MeV with an RFQ and the 200 MHz LINAC with an efficiency of about 50%. The pulse of H^- ions is strip-injected and captured into a single bunch in the AGS Booster. The bunch in the Booster will then contain about $N_B = 4 \times 10^{11}$ polarized protons with a normalized 95% emittance of about $\pi\varepsilon_N = 10\pi$ μm. The single bunch of polarized protons is accelerated in the Booster to 1.5 GeV kinetic energy and then transferred to the AGS, where it is accelerated to 25 GeV.

2.1. Polarized ion source

The new RHIC optically pumped polarized H^- source (OPPIS) was constructed at TRIUMF from the KEK OPPIS source [10]. The goal of providing at least 0.5 mA H^- ion current with 80% polarization during a 300 μs pulse, within a normalized emittance of 2π μm has been achieved. This is an ideal application for the ECR-type OPPIS. A pulsed laser is used to optically pump the rubidium vapor.

2.2. Acceleration in the booster and AGS

During acceleration, the polarization may be lost when the spin precession frequency passes through a depolarizing resonance. The two weak resonances in the Booster ($G\gamma = 3$ and 4) are easily corrected by a harmonic correction of the closed orbit, since there are only two of them.

Traditionally, the depolarizing resonances in the AGS were corrected by the tedious harmonic correction method for the imperfection resonances and by a tune jump method for the intrinsic resonances [11]. In recent years a few new methods have been used to cross depolarizing resonances in the AGS. A 5% (rotation of 9° around the longitudinal direction) partial Siberian Snake [12] has been added to one of the straight sections in the AGS. A 5% Snake is sufficient [13] to avoid depolarization due to the imperfection resonances without using the harmonic correction method. As predicted the polarization reverses sign whenever $G\gamma$ is equal to an integer. Since the partial snake is a solenoid, it does introduce some coupling. A fast tune jump has been used along with the partial snake to cross resonances and enabled the beam to be accelerated up to 25 GeV while retaining some polarization. However, a significant amount of polarization while crossing the intrinsic resonances $G\gamma = 0 + \nu_y$, $12 + \nu_y$, and $36 + \nu_y$.

Full spin flip can be achieved with a strong artificial RF spin resonance excited by an RF dipole [14] at a modulation tune ν_m. If we choose the RF spin resonance location $K_{RF} = n \pm \nu_m$ near the intrinsic spin resonance, the spin motion will be dominated by the RF resonance and the spin near the intrinsic resonance will adiabatically follow the spin closed orbit of the RF spin resonance. This method is different than simply enhancing the intrinsic resonance which also enhances the coupling resonance strength as has been proposed earlier [15]. Fig. 2 shows the new record proton beam polarization achieved during a run of the E-880 experiment. The RF dipole was used to completely flip the spin at the four strong intrinsic resonances $0 + \nu_y$, $12 + \nu_y$, $36 - \nu_y$, and $36 + \nu_y$. The lower curve shown going through the data points was obtained from a spin tracking calculation simulating the experimental conditions. Most of the residual polarization loss is caused by the coupling resonances. A new AGS partial Snake using a helical dipole magnet would eliminate all coupling resonances [16]. Spin tracking simulations of this condition are depicted by the upper curve in Fig. 2. The depolarization from the two weak intrinsic resonances $24 + \nu_y$ and $48 - \nu_y$ could be avoided using an energy jump method described above.

At 25 GeV, the polarized protons are transferred to RHIC. At this energy the transfer line between the AGS and RHIC is spin transparent

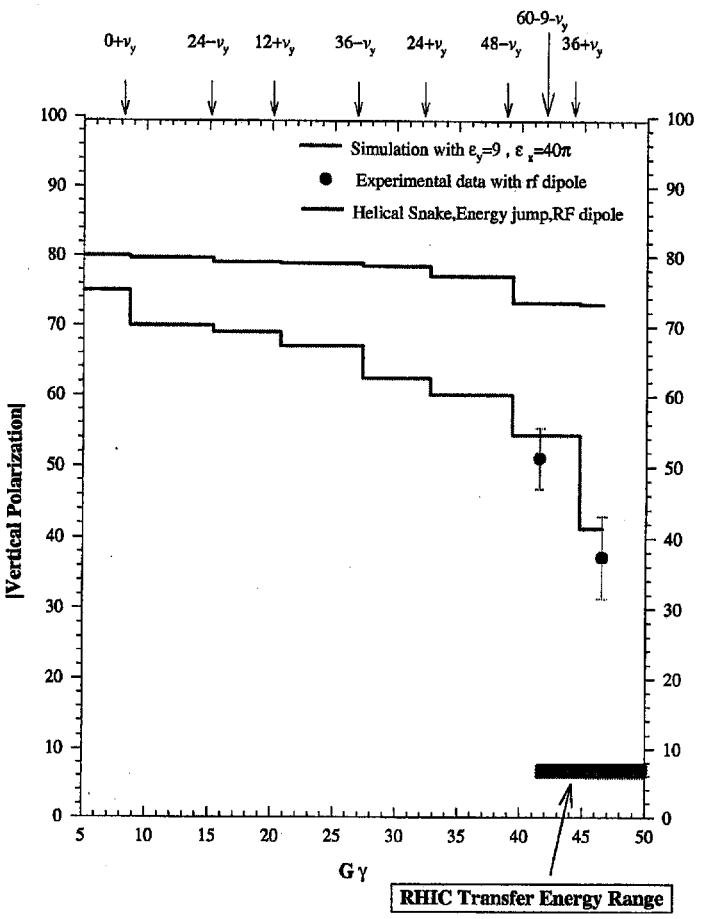

Fig. 2. Vertical polarization versus $G\gamma$ measured during the November 1997 run of E-880. The lower curve is the result of a spin tracking calculation for the experimental conditions. The upper curve simulates the use of a helical partial Snake in the AGS.

[17]. If the last resonance, $G\gamma = 36 + \nu_y$, cannot be crossed without significant polarization loss it is possible to transfer the polarized protons to RHIC before crossing this resonance in the AGS at an energy of 22.4 GeV ($\gamma \approx 25$). This is discussed in the following section.

We estimate that the overall efficiency of the acceleration and beam transfer is better than 50%, giving 2×10^{11} protons per bunch. With proper care the normalized emittance of the bunch is expected to be much less than 20π μm. A vertical beam emittance less than 10π μm has been achieved in past studies. We repeat the process until all 120 bunches of each ring are filled. Since each bunch is accelerated independently, we have the option of preparing the polarization direction of each bunch independently. Filling both RHIC rings with 120 bunches each and accelerating to full energy will only take about 10 minutes which is short compared to the expected lifetime of the stored polarized proton beams in RHIC of many hours.

3. AGS-to-RHIC transfer line

The AGS to RHIC (AtR) transfer line [18] has been designed to transport proton beams in the

energy range, from 20.58 GeV (just above the RHIC transition Energy) to a maximum injection energy of 28.3 GeV. The range of energies for transfer of polarized beam is more restricted, since there are interleaved horizontal and vertical bends in the transport line.

3.1. AtR sections affecting the proton beam polarization

The layout of the (AtR) transfer line is shown in the schematic diagram of Fig. 3. In the AtR transfer line there are two sections of the beam line where the beam direction is not parallel to the horizontal plane but makes an angle below the horizontal plane. The first of the sections is located in the W-line within the 20° bend. The second section is located at the end of the X or Y-lines in the RHIC injection section.

The vertical drop at the 20°-bend consists of a −12.51 mrad vertically bending magnet located after the second horizontally bending magnet of the 20° W-line [18] (see Fig. 4) followed by six combined-function dipole magnets which bend the beam horizontally to the right by 15°, and finally a +12.46° mrad vertically bending dipole which restores the beam direction to the horizontal plane.

A schematic diagram of the vertical bends near the injection point is shown in Fig. 5. The beam is injected vertically into each of the RHIC rings. For the Yellow ring (CCW), in the injection region the vertical displacement begins with a −3.0 mrad vertically bending magnet followed by a Lambertson septum magnet [19] which bends the beam 38.0 mrad to the right, then a RHIC quadrupole (vertically defocusing)—dipole (left-bend)—quadrupole (vertically focusing) and finally the vertically bending RHIC injection kicker which deflects the beam by +1.73 mrad which restores the

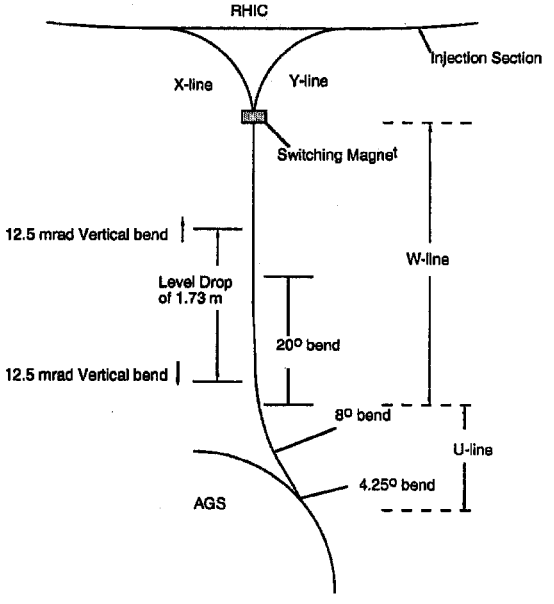

Fig. 3. Schematic diagram of the AGS to RHIC (AtR) transfer line. The 12.51 mrad vertical bend is located at the region of the 20° horizontal bend. The 3 mrad bend is located at the end of the RHIC injection section shown in the figure.

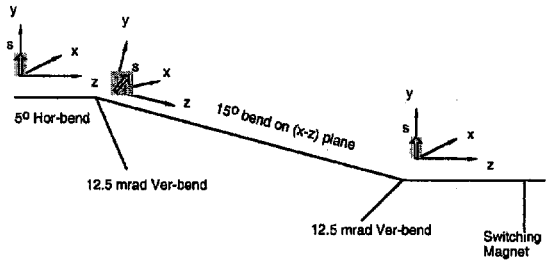

Fig. 4. Schematic diagram of the "12.5 mrad vertical bend". A −12.51 mrad vertical bend is followed by a 15° horizontal bend and +12.46° vertical bend. (Note that the small difference in vertical bends is used to correct for the earth's curvature.)

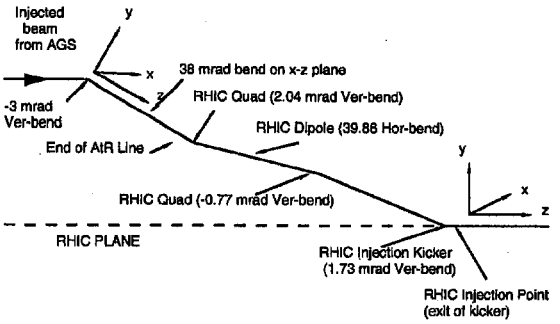

Fig. 5. Schematic diagram of the "3.0 mrad vertical bend". The beam is injected off axis with respect to the two RHIC quadrupoles which act also as vertical bending magnets. This injection geometry reduces the required strength of the vertical injection kicker, to a value of 1.73 mrad.

injected beam onto the RHIC plane. The strength required for the vertical injection kicker to restore the beam back to the horizontal plane has been reduced down to 1.73 mrad because part of the vertical bend has been accomplished by the two RHIC quadrupoles. (For the injection into the Blue (CW) ring, the polarity of both, the Lambertson injection magnet and RHIC dipole have to be inverted.) The exit point of the RHIC injection kicker is defined here as the "RHIC injection point." It is the arrangement of the bending magnets in these two vertical bends (vertical bend followed by horizontal bend and then vertical) that affects the stable spin direction of a polarized proton beam.

The stable spin direction of a polarized proton beam circulating in RHIC which will operate with two full Snakes, is along the vertical. Therefore the stable spin direction of the injected polarized beam should be along the vertical if possible. Optimization of the spin transport was found to be best if the extraction from the AGS occurs at $G\gamma = n + \frac{1}{2}$. Fig. 6 shows the relative injected vertical polarization for different RHIC injection energies. Transmission is better than 95% for $G\gamma > 45.5$.

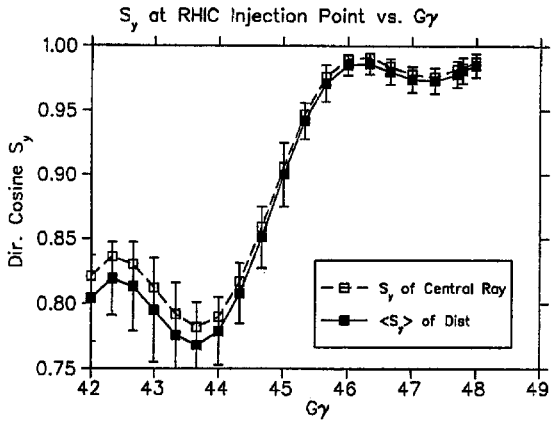

Fig. 6. The S_y component of the stable spin direction at the RHIC injection point. The empty squares correspond to the central trajectory particle. The filled squares to the average S_y of the spin distribution. The error bars correspond to one standard deviation of the S_y component of the spin distribution. The initial spin direction at AGS has been assumed vertical. (AGS Snake off.)

4. Snakes and spin rotators in RHIC

To fit within existing straight sections in RHIC, it is important to find the most compact design for Siberian Snakes and Spin Rotators which could produce the desired spin rotation in the shortest space and with minimal orbit excursions. A particularly elegant solution was proposed by V. Ptitsin and Y. Shatunov [20]. Their solution is based on helical dipole magnet modules, each having a complete 360° twist. Using helical dipole magnets minimizes orbit excursions which are most severe at injection energy. This allowed for a more modular design, where similar superconducting helical magnets could be used for both Snakes as well as Spin Rotators near the interaction points in RHIC.

4.1. General layout

Two full Siberian Snakes on opposite sides of each of the two RHIC rings serve to avoid depolarization from imperfection and intrinsic depolarizing resonances up to the top energy of 250 GeV. In addition, spin rotators are required at the intersection points used by PHENIX and STAR to allow for measurements of spin effects with longitudinally polarized protons. The spin rotators rotate the polarization from the vertical direction into the horizontal plane on one side of the interaction region and restore it to the vertical direction on the other side.

The Siberian Snakes introduce a 180° spin rotation without generating a net orbit distortion. The spin rotators placed around the experiments rotate the spin by 90° to provide longitudinal polarization at the interaction region again without generating net orbit distortions. In both cases the spin rotation is accomplished with a sequence of constant field, superconducting helical dipole magnets.

Each Snake rotates the spin by 180° around a horizontal axis and the two axes of the two Snakes of each ring have to be perpendicular to each other. We use pairs of Siberian Snakes with one Snake rotating the spin around an axis that points 45° to the outside and the other Snake rotating around an axis that points 45° to the inside of the

ring. In this case all Snakes could be constructed in the same way. Also, the two Snakes of each ring have to be installed on opposite sides of the ring. In fact, the beam direction in one Snake has to be exactly opposite to the beam direction in the other Snake to within 0.3 mrad. The following is a summary for the locations and construction of the Siberian Snakes and the spin rotators (see Fig. 7):

- Two pairs of full Siberian Snakes, one pair in each ring, are installed in the 3 o'clock and 9 o'clock sections of RHIC as shown in Fig. 1. These Snakes rotate the spin around axes that point 45° to the inside or outside of the ring. We installed the Siberian Snakes in the 13 m long, cold straight sections between Q7 and Q8.
- The two pairs of spin rotators, one set for PHENIX at the 8 o'clock region and another set for STAR at the 6 o'clock region, are installed in the 40 m long straight sections between Q3 and Q4 on either side of the interaction region. The beam direction in the straight sections is different from the direction in the collision area by 3.67 mrad which introduces a spin rotation that is larger by a factor of $G\gamma$. This means that the Spin Rotators have to prepare a horizontal polarization direction such that after this spin rotation the

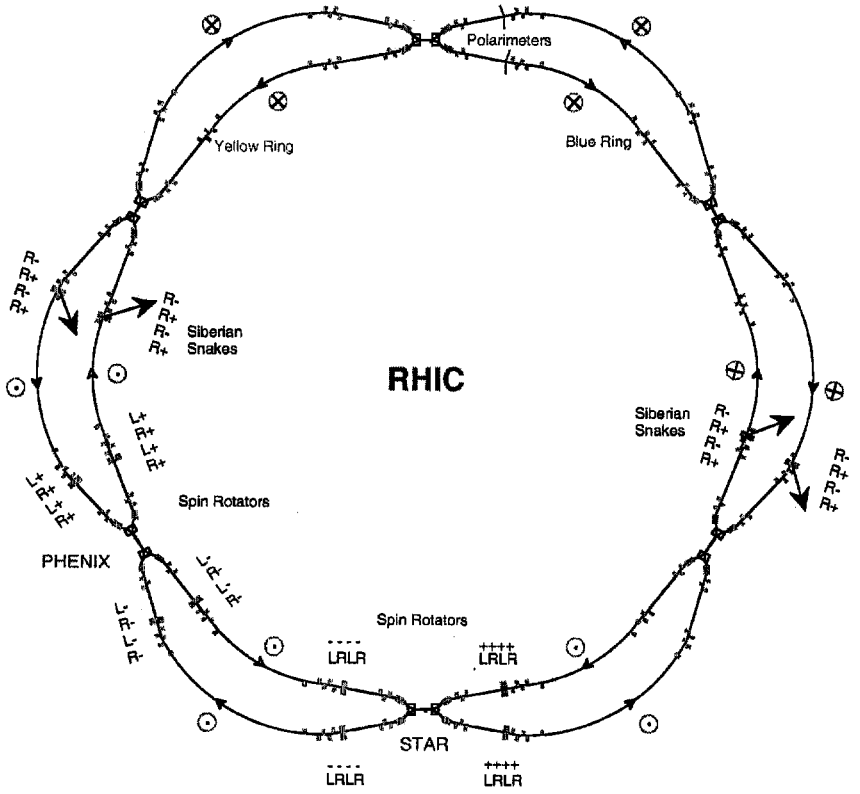

Fig. 7. View of RHIC overemphasizing the interaction regions to show the location of the Siberian Snakes and the spin rotators placed around the collider experiments STAR and PHENIX. Also shown are the polarization directions around the rings and around the detectors for collisions with longitudinal polarization.

desired longitudinal polarization direction is obtained at the interaction point.

4.2. Siberian Snake and spin rotator design

Each snake and rotator is composed of four helical dipole magnets [20]. Helical field magnets have some distinctive advantages over more conventional transverse Snakes or rotators: (i) the maximum orbit excursion is smaller, (ii) orbit excursion is independent from the separation between adjacent magnets, and (iii) they allow an easier control of the spin rotation and the orientation of the spin precession axis.

In an ideal helical dipole magnet to be used for our purposes, the central dipole field should rotate through a complete 360° from one end of the magnet to the other. In a real magnet, of course, the fields at the ends of the magnet will also contribute to the particle dynamics. We require that the integrals $\int B_x \, d\ell$ and $\int B_y \, d\ell$ are both less than 0.05 Tm. The maximum body field will thus rotate through an angle less than 360° along the axis of the magnet. Moreover, in order to simplify the construction of the Snakes/rotators, a solution has been found with all magnetic modules identical in both devices. For the snakes each helix is right handed with the field at the end being vertical. For the rotators, the helices alternate between right and left handedness (see Fig. 7) with the field at the end of each helix being horizontal.

The orbit though a ideal helix will have the incoming and outgoing rays parallel, but transversely displaced. In order to have a net displacement of zero through a snake we require that the offset be canceled by powering in pairs with opposite fields. The inner pair are wired in series with opposite polarity and powered by a common power supply. The outer pair are also wired in series with opposite polarity to a second supply. Fig. 8 shows the field components, design orbit, and spin rotation through the a snake at injection

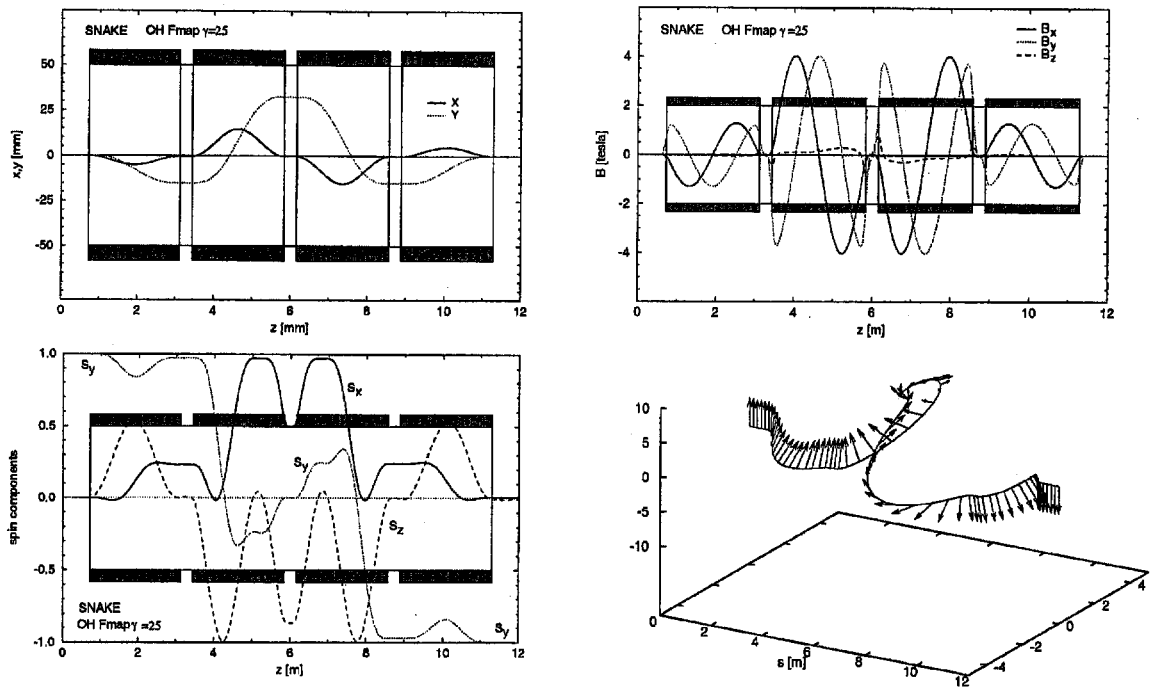

Fig. 8. Field, orbit, and spin tracking through the four helical magnets of a Siberian Snake at $\gamma = 25$. The spin tracking shows the reversal of the vertical polarization.

energy. At 250 GeV the required fields are almost the same, but the orbit displacement in the middle of the snake is only about 3 mm.

By operating the helices at different currents it is possible to adjust both the amount of spin rotation (angle μ) and axis of rotation. With the helices wired as described above, the axis of rotation for the snake is in the horizontal plane at an angle ϕ from the longitudinal direction. Fig. 9 shows the dependence of μ and ϕ on the two field settings—B_1 for the outer pair of helices, and B_2 for the inner pair.

Snake parameters are listed in Table 1. The parameters are a result of an optimization using an orbit and spin tracking program that includes the effects of fringe fields [21,22]. The integration is performed by interpolation through the magnetic field numerically calculated and mapped on a three-dimensional grid. The result of the orbit and spin tracking is shown in Fig. 8. To produce these results, it was found that the central body field of the helical magnets should rotate through approximately 340°, with the ends contributing the necessary remaining field. Naturally, the exact amount of rotation depends upon the model used to describe the ends, and final magnet parameters will be a result of actual magnet tests and measurements.

Spin rotator parameters are listed in Table 2. The result of the orbit and spin tracking is shown in Fig. 10. Since in RHIC the direction of the spin rotator beam line is at a horizontal angle $\theta = 3.674$ mrad with the direction of the adjacent insertion, the spin should emerge from the rotator in the horizontal plane and at an angle $G\gamma\theta$ with the rotator axis in order to obtain a longitudinal polarization through the insertion region. The needed rotation is therefore dependent on the beam energy. The values of the field needed to provide a longitudinal polarization at different energies are shown in Fig. 11. The rotators will be turned on only after accelerating the beam to the desired storage energy.

4.3. *Effects on RHIC operation*

Calculations of the changes to the RHIC lattice parameters generated by the helical dipole magnets

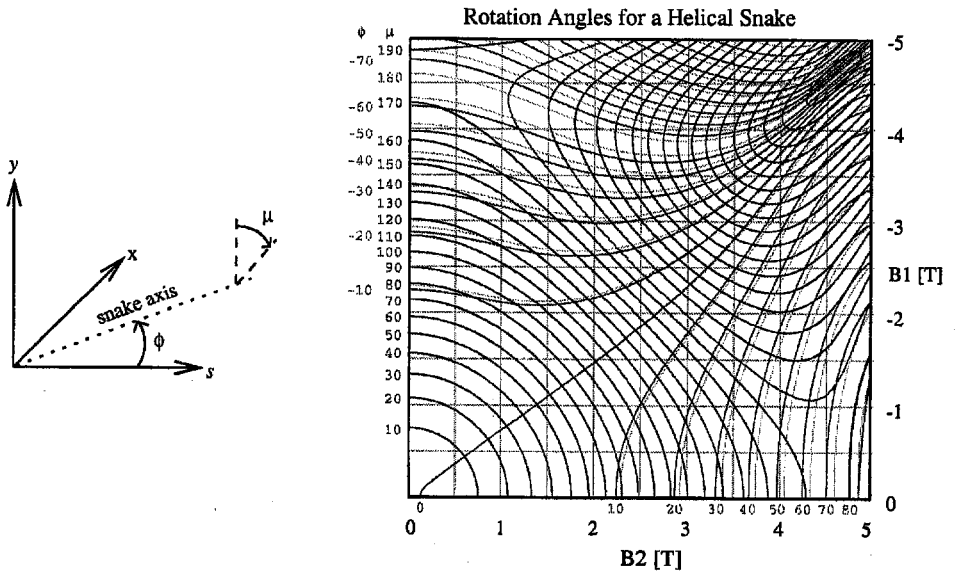

Fig. 9. Change of the direction of the Snake rotation axis as a function of magnet excitation. This calculation uses a simplified analytical expression for the Snake magnetic field. The rotation axis of the snake is ϕ, and μ is the rotation angle. Note that the ϕ contours shift slightly from injection (red) at 25 GeV to storage (pink) at 250 GeV. B_1 is the field strength of the outer pair of helices, and B_2 is the field strength of the inner pair.

Table 1
Parameters for the Siberian Snake magnets. All helical magnets are right-handed, and begin and end with vertical fields. The central field strengths were optimized to include end effects of the magnets

Number of helical magnets	4
Total length	10.56 m
Magnet bore	100 mm

Helical magnets

	Length (effective)	Field helicity	Field orientation at entrance/exit	Field strength
1	2.40 m	right-handed	Vertical	1.3 T
2	2.40 m	right-handed	Vertical	−4.0 T
3	2.40 m	right-handed	Vertical	4.0 T
4	2.40 m	right-handed	Vertical	−1.3 T

Max. orbit excursion (hor./ver.)	(25 GeV)	15 mm/33 mm
Total field integral		24 T-m
Orbit lengthening	(25 GeV)	2 mm

Table 2
Parameters for the Spin Rotator magnets. Helical magnets alternate right-handed and left-handed, and all begin and end with horizontal fields. The central field strengths were optimized to include end effects of the magnets, and are calculated for longitudinal polarization at the beam collision point

Number of helical magnets	4
Total length	10.56 m
Magnet bore	100 mm

Helical magnets

	Length (effective)	Field helicity	Field orientation at entrance/exit	Field (25 GeV)	Field (250 GeV)
1	2.40 m	right-handed	Horizontal	2.1 T	3.5 T
2	2.40 m	left-handed	Horizontal	2.8 T	3.1 T
3	2.40 m	right-handed	Horizontal	2.8 T	3.1 T
4	2.40 m	left-handed	Horizontal	2.1 T	3.5 T

Max. orbit excursion (hor./ver.)	(25 GeV)	25 mm/10 mm
Total field integral		23 T-m
Orbit lengthening	(25 GeV)	1.4 mm

show minimal effects on the RHIC lattice parameters. Because of the spiral trajectory within the magnets, the Snakes and rotators introduce coupling into the RHIC accelerators. Both computer modeling and analytical calculations have shown that this effect is also small, with a minimum tune separation due to coupling of $\Delta v = 0.004$ with two Snakes and 4 Spin Rotators present at RHIC injection [23,24].

The effects on RHIC operation of helical dipole magnet error fields and misalignments have also been studied [25]. In contrast to a "regular" dipole magnet error which can be thought of as producing a kink in the slope of the particle trajectory at

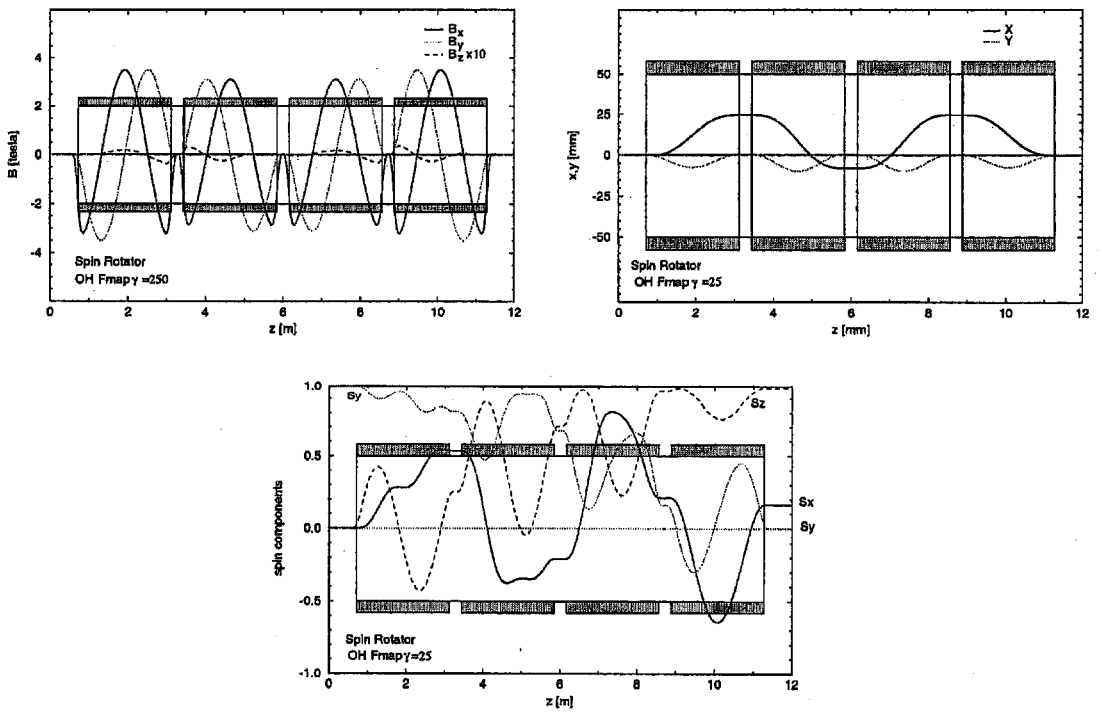

Fig. 10. Field, orbit, and spin tracking through the four helical magnets of a Spin Rotator at $\gamma = 25$. In this example, the spin tracking shows how the polarization is brought from vertical to horizontal.

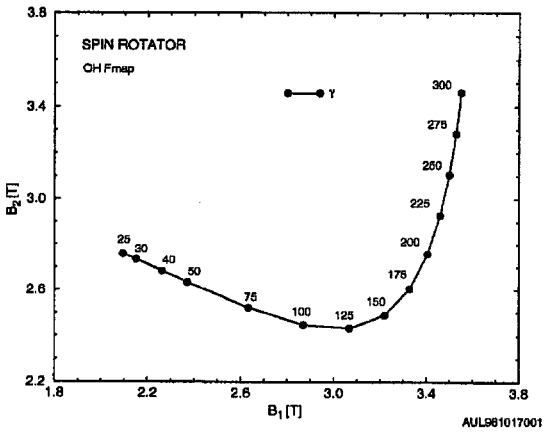

Fig. 11. Excitation of the two pairs of helical magnets in the rotator to achieve longitudinal polarization in the insertion of RHIC, for various beam energies.

the source of the error, a "helical dipole" error will introduce a step in the trajectory. To keep the vertical orbit distortions under control, the helical dipole field errors $\Delta(B\ell)/(B\ell)$ should be kept reasonably below 1%, and rotational misalignments should be less than about 10 mrad. The more important parameter will be the total integrated field strength ($\int B_x \, ds, \int B_y \, ds$) which should be zero, or equivalently the total equivalent integrated twist of the magnet should be 360°. This last requirement is especially sensitive in the case of the Rotator magnets (horizontal fields at the entrance and exit of the magnets). The Rotators, however, are only used at storage energy, where their effects on the orbit are smaller. With two Snakes on throughout injection and acceleration, the orbit distortions generated by their twist errors can easily be corrected using standard RHIC dipole correctors. The total twist angle and its tolerance are $360° \pm 2°$ [26]. The ends of the magnets have been carefully designed to obtain not only the desired integrated field strength but also the desired total field twist well within this tolerance [27,28].

Field quality is also an issue for the helical magnets, though not as central an issue as for the normal bending magnets in the accelerator. The intrinsic helical nature of the field will itself produce nonlinear terms in the field expansion. In particular, Maxwell's equations dictate that the helical dipole field will be of the form

$$B_x \approx -B_0\left\{\left[1+\frac{k^2}{8}(3x^2+y^2)\right] \times \sin kz - \frac{k^2}{4}xy\cos kz\right\} \quad (4)$$

$$B_y \approx B_0\left\{\left[1+\frac{k^2}{8}(x^2+3y^2)\right] \times \cos kz - \frac{k^2}{4}xy\sin kz\right\} \quad (5)$$

$$B_z \approx -B_0 k\left\{1+\frac{k^2}{8}(x^2+y^2)\right\} \times [x\cos kz + y\sin kz] \quad (6)$$

where the repeat period of the helical field is $\lambda = 2\pi/|k|$. In the above, we have assumed a field which is "vertical" (i.e., positive y direction) at the entrance to the magnet. The sign of k determines the handedness of the field. To first order, the transverse fields are just $B_y = B_0 \cos kz$, $B_x = -B_0 \sin kz$ as desired. However, we see that for significant displacements, there are nonlinear terms which will contribute to the particle motion.

In addition to this intrinsic nonlinear feature, magnet design and construction errors will add nonlinearities to the field as well. While the nonlinear field components tend to average to zero over the length of the helical dipole, the protons follow a trajectory which is not centered within the magnet. (This is illustrated in Fig. 8, in which the choice of the name "Snake" is readily apparent.) Thus, one expects to see feed-down effects due to this trajectory. For example, a sextupole component in the magnet will generate a tune shift due to the off-centered orbit. Analytical estimates indicate that the intrinsic tune shift at 25 GeV due to two Snakes in RHIC is on the order of $\Delta\nu \approx 0.015$, and that a sextupole component in the magnet design of strength $b_2 \approx 2 \times 10^{-4}/\text{cm}^2$ (or, approximately 20 "units" measured at 3.1 cm) will give approximately the same tune shift [29,30]. Particle tracking results are in qualitative agreement with these estimates [31]. For a discussion of measurements of actual helical dipoles see Refs. [7,8]. Parameters and tolerances for magnets are given in Table 3.

4.4. *Compensation for detector solenoids*

The STAR and PHENIX detectors use solenoid magnets as spectrometers. With transverse polarization at the collision point the solenoid

Table 3
General parameters and tolerances for an individual Snake or Rotator magnet. Magnet multipole coefficients are in units of 10^{-4} cm^{-n}

Parameter		Requirement
Design central field	B_0	4 T
Operating margin		15 %
Design magnetic length	$\frac{1}{B_0}\int \lvert B\rvert \, dL$	2.40 m
Total cryostat assembly length		11.87 m
Integrated field strength	$\int \lvert B\rvert \, d\ell$	9.6 ± 0.05 T · m
Integrated field components	$\int B_x \, d\ell$, $\int B_y \, d\ell$	0 ± 0.05 T · m
Quadrupole coefficient of main dipole field	b_1	0 ± 2.0
Sextupole coefficient of main dipole field	b_2	2.0 ± 2.0
Octopole coefficient of main dipole field	b_3	0 ± 2.0
Decapole coefficient of main dipole field	b_4	2.0 ± 1.0
Skew quadrupole coefficient of main dipole field	a_1	0 ± 2.0
Transverse alignment[a]	$\Delta x, \Delta y$	0 ± 0.5 mm
Longitudinal alignment[a]	Δz	0 ± 10 mm
Rotational alignment[a]	$\Delta\phi$	0 ± 1.0 mrad

[a] Alignment is with respect to neighboring quadrupoles.

contributes to the imperfection resonance strength,

$$\varepsilon_{\mathrm{imp,sol}} = \frac{1+G}{2\pi}\frac{\int B_{\parallel}\,\mathrm{d}\ell}{B\rho}. \tag{7}$$

For a 5 tesla-meter integrated solenoid field strength, the resulting spin resonance strength is about 0.02 at the injection energy and 0.003 at 250 GeV/c.

With longitudinal polarization at the collision point the longitudinal field rotates the polarization around its axis and thus changes the spin tune. The spin tune is changed by 0.03 to 0.003 at 25 and 250 GeV, respectively, by a 5 T m solenoid. This can be compensated by adjusting the direction of the axes around which the Snakes rotate the spin. By adjusting up to $\pm 5°$ the spin tune can be adjusted for energies down to 25 GeV.

5. Polarized proton acceleration in RHIC

5.1. Depolarizing resonance strengths

Without Siberian Snakes there are numerous depolarizing resonances in RHIC, both intrinsic and imperfection resonances. The strengths of the intrinsic resonances can be calculated quite accurately from the appropriate integral over the horizontal focusing fields. Fig. 12 shows the result for the RHIC lattice with $\beta^* = 10$ m at all intersections. A calculation with $\beta^* = 1$ m gave only a slightly different result. The calculation was performed for a particle with a normalized Courant–Snyder invariant of $\epsilon_0 = 10\pi$ mm mrad. For a different value of the invariant the strength scales according to

$$\varepsilon = \varepsilon_0\sqrt{\frac{\epsilon}{\epsilon_0}} \tag{8}$$

where ε_0 is the resonance strength for the invariant ϵ_0.

Important intrinsic spin resonances are located at

$$G\gamma = kP \pm \nu_y \approx mPM \pm \nu_{\mathrm{B}} \tag{9}$$

where k and m are integers, P is the superperiodicity of the accelerator, M is the number of FODO cells per superperiod, and $2\pi\nu_{\mathrm{B}} = 2\pi(\nu_y - 12)$ is the accumulated phase advance of all FODO cells, which contain bending dipoles.

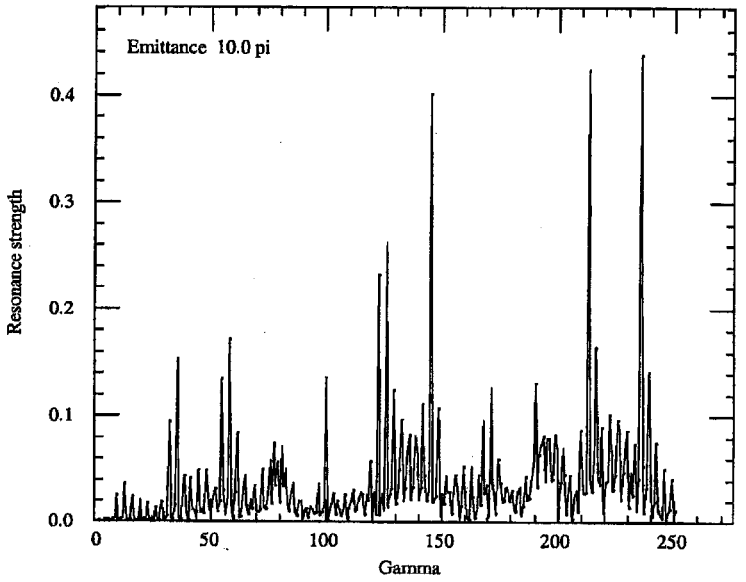

Fig. 12. Strengths of the intrinsic depolarizing resonances in RHIC calculated for the RHIC lattice and for both $\beta^* = 10$ m and 1 m at all six intersection points. There is no noticeable difference of the calculated strengths for the two values of β^*.

The locations of the three strongest intrinsic resonances are approximately at

$$G\gamma = 3 \times 81 + (\nu_y - 12), \quad 5 \times 81 - (\nu_y - 12), \quad 5 \times 81 + (\nu_y - 12) \tag{10}$$

$$\gamma = 145, 216, 235 \tag{11}$$

where 81 is the product of superperiodicity, 3, and the "effective" FODO cells per superperiod, 27, which includes dispersion suppressors. The strengths of all 3 strong resonances are less than 0.5.

Important imperfection resonances are located at an integer closest to strong intrinsic resonances. This is clearly shown in the top part of Fig. 13 which shows the calculated imperfection resonance strengths for an uncorrected closed orbit obtained from a random sample of magnet misalignments with a rms spread of ± 0.5 mm, dipole roll angles with a spread of ± 1 mrad, dipole field errors of $\pm 5 \times 10^{-4}$, and position monitor errors of ± 0.5 mm. After the closed orbit correction scheme MICADO [32] was applied, the vertical closed orbit was corrected to within 0.155 mm rms. The resonance strengths are greatly reduced as shown in the lower part for Fig. 13. The strengths of the imperfection resonances generally increase linearly with the beam energy and are bounded by

$$\varepsilon_{\text{imp}} = 0.25 \frac{\gamma}{250} \sigma_y \tag{12}$$

where σ_y is the rms value of the residual closed orbit excursions in mm. The strength is smaller than 0.04 for all energies. Present alignment data from the RHIC CQS cold masses has shown monitor and quadrupole placement errors each well below 0.5 mm. The dipole roll angle is well below 0.5 mrad as well [33].

5.2. *Effectiveness of Siberian Snakes*

With the installation of Siberian Snakes, which are local 180° spin rotators, the spin tune becomes 1/2, independent of the beam energy. Clearly the depolarizing resonance conditions cannot be met anymore as long as the fractional betatron tune $\Delta\nu_y \neq 1/2$ and therefore, in principle, no depolarization would occur. This is in fact true as long as the depolarizing resonances are not too strong. However, in the presence of strong resonances depolarization can occur from resonance conditions extended over more than just one turn. This leads to additional possible depolarizing resonance conditions:

$$\Delta\nu_y = \frac{\nu_{\text{sp}} \pm k}{n}. \tag{13}$$

They are called Snake resonances [34] and n, the number of turns, is called the Snake resonance order. For two Snakes, as proposed here for RHIC, significant depolarization from Snake resonances only occurs for an intrinsic resonance strength of about 0.5 and even order Snake resonances require in addition an imperfection resonance strength of about 0.05. Fig. 14 shows the result of a simple 1-D spin tracking calculation through an energy region (using the RHIC acceleration rate) with an intrinsic resonance of strength 0.5 and an imperfection resonance of strength 0.05. There are clearly regions of the betatron tune that do not experience any depolarization. Since the betatron tunes of RHIC were chosen to be located between 1/6 and 1/5, the betatron tune could be placed between the Snake resonances $1/6 = 0.1667$ and $3/16 = 0.1875$. With the betatron tune including its spread located between 0.170 and 0.185, a 0.015 range, no depolarization will occur over the whole RHIC energy range up to the top energy. A more detailed discussion of spin resonances and acceleration is given in Ref. [1].

5.3. *Spin reversal of stored beams*

Since the proposed asymmetry measurements are high precision measurements, frequent polarization sign reversal is imperative to avoid systematic errors. Possible sources for systematic errors are luminosity variations, crossing angle variations, and detector efficiency variations. As mentioned earlier different bunches will have different polarization signs and therefore different bunch crossings will measure interactions with different combinations of incoming beam polarization signs. Although this will greatly reduce systematic errors it is still true that one pair of bunches would always cross with the same

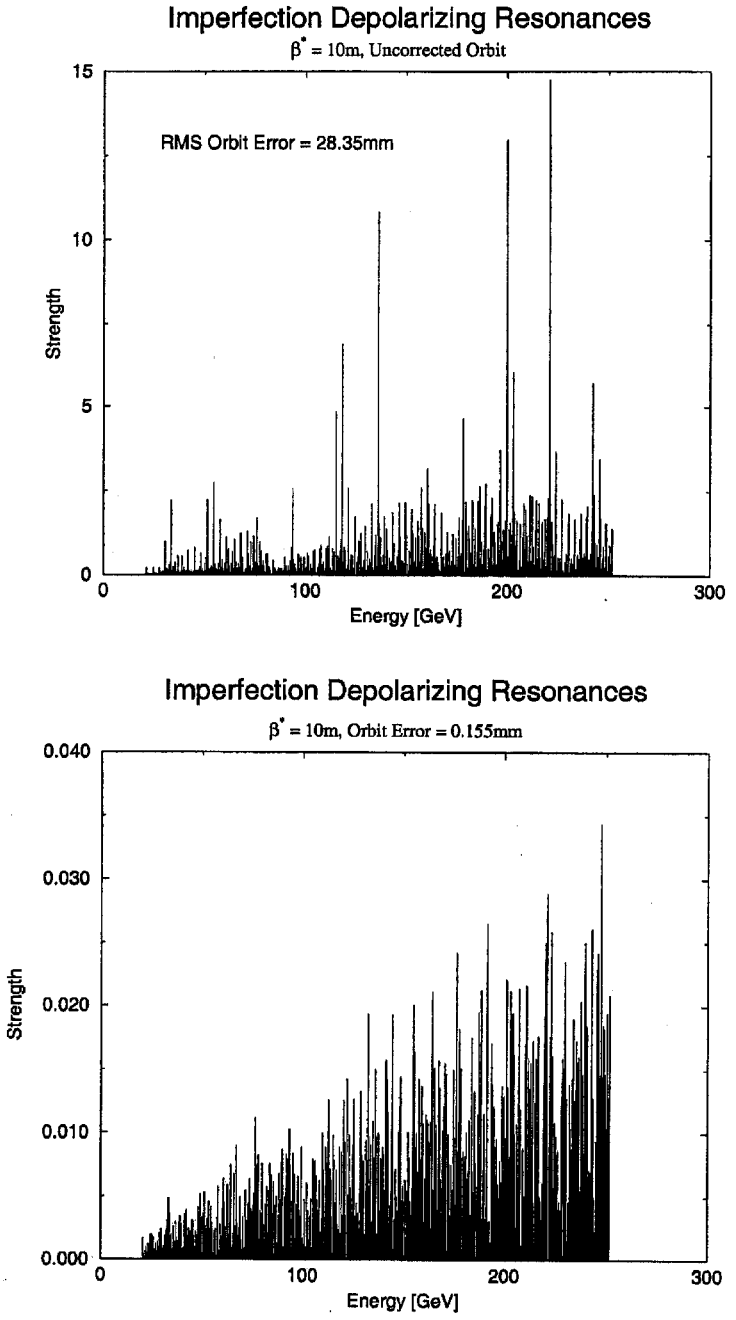

Fig. 13. Strengths of the imperfection depolarizing resonances in RHIC calculated before and after the MICADO orbit correction scheme has been applied.

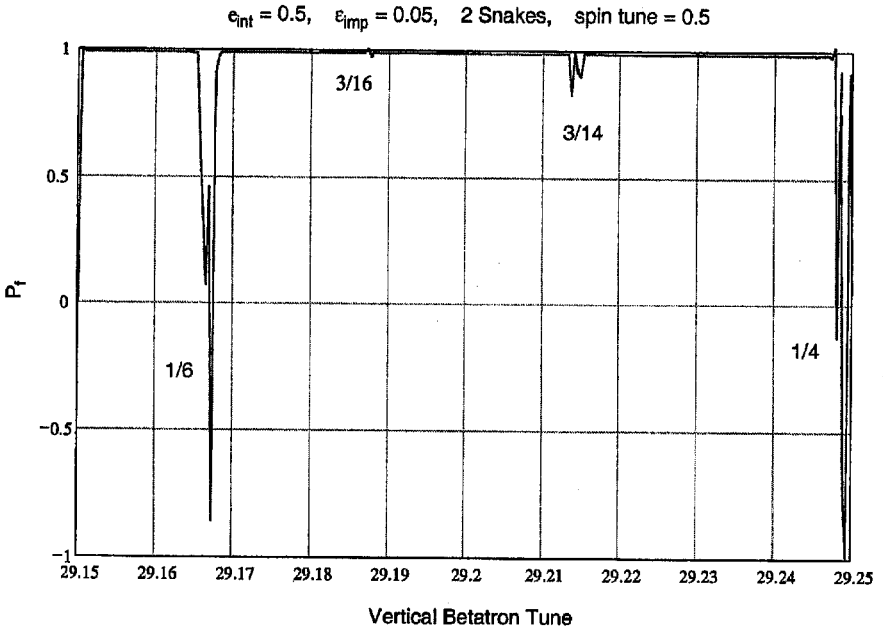

Fig. 14. Vertical component of the polarization after acceleration through a strong intrinsic resonance and a moderate imperfection resonance shown as a function of the vertical betatron tune.

combination of polarization signs during the whole lifetime of the stored beams which is at least several hours. To eliminate the possibility of systematic errors from this situation we propose to install a spin flipper in each ring which is capable of reversing the polarization sign of all bunches. The spin flippers consist of vertical dipole magnets [35] excited with about 40 kHz AC current. This would drive an artificial spin resonance which can be used to adiabatically reverse the polarization direction.

We estimate that complete spin reversal would take less than 1 s. The same device will be used to accurately measure the spin tune by measuring the spin reversal efficiency as a function of the frequency of the spin flipper excitation. This is instrumental to adjust the spin tune to 0.500.

In most cases such a simple oscillating driving field is very effective in driving an artificial resonance since the oscillating field can be thought of as the sum of two counter-rotating fields, only one of which is in resonance with the beam precession frequency. However, with a Snake the spin tune is a half-integer and therefore the two counter-rotating fields are both in resonance and interfere so that effectively only half of the beam around the ring circumference sees a driving field. By designing a true rotating field the beam polarization can be fully flipped even with a half-integer spin tune.

Several designs have been proposed, all involving two sets of AC magnets with a 90° phase difference between them. The first design uses

Table 4
Parameters for a spin flipper that produces a true rotating driving field. The excitation of the AC magnets indicates the relative phase shift between the four magnets

Magnet	Strength	Excitation
1. Vertical magnet	0.01 Tm	$\sin \omega t$
2. Horizontal magnet	+4.2 Tm	DC
3. Vertical magnet	0.01 Tm	$-2 \sin \omega t + \cos \omega t$
4. Horizontal magnet	−8.4 Tm	DC
5. Vertical magnet	0.01 Tm	$\sin \omega t - 2 \cos \omega t$
6. Horizontal magnet	+4.2 Tm	DC
7. Vertical magnet	0.01 Tm	$\cos \omega t$

three strong DC magnets interleaved with four independently driven vertical AC magnets. Table 4 shows the parameters of such a spin flipper, which could fit into a regular 12 m straight section. The DC magnets in this first design are quite strong and expensive. A less expensive design would utilize one of the two Siberian Snakes instead of special DC magnets. The two sets of vertical AC magnets are placed symmetrically around the Snake with one set generating a vertical bump of half a vertical betatron wavelength and the other one a full wavelength long. By driving the bumps with 40 kHz AC 90° out of phase a rotating driving field will be generated. Alternatively, and also least expensively, the spin tune can be simply moved away from the value of 0.5 during the spin flip operation using the tunability of the Snakes. To achieve full spin flip with less than 0.01% polarization loss per flip a field integral for the AC magnet of $\int B\,\mathrm{d}l = 0.01$ Tm and a flip time of about 1.0 s is required [36].

To avoid emittance growth from the oscillating vertical deflections, the dipole needs to be turned on and off slowly (adiabatically) as shown in Fig. 15. This scheme was successfully tested in the AGS where adiabatic build up of betatron oscillation amplitudes in excess of two beam sigma, and subsequent adiabatic turn off, has been demonstrated without emittance growth [37].

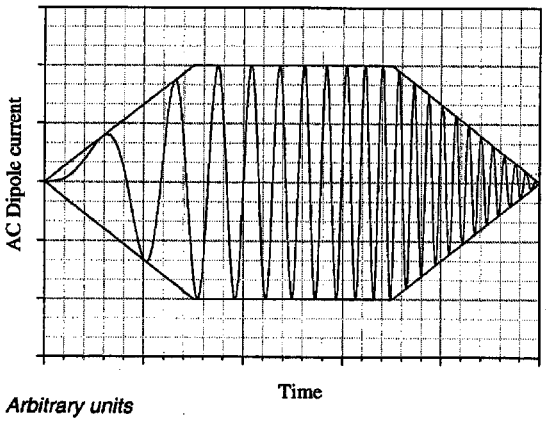

Fig. 15. Schematic diagram of the excitation dipole current as a function of time. Note the increase of frequency with time. The trapezoidal lines are the amplitude envelopes to guide the eye.

6. Measuring beam polarization in RHIC

Our approach of measuring the beam polarization is based on the asymmetry in proton-Carbon elastic scattering in the Coulomb-Nuclear Interference (CNI) region. It is expected that the relative beam polarization can be determined by using a pC CNI polarimeter to 10% for each measurement in seconds at full luminosity. The future addition of polarized proton jet target will allow us to calibrate the pC CNI polarimeter to 5%.

6.1. Introduction

In general, vertical beam polarization is measured by determining the asymmetry in the cross section for left and right scattering or particle production, using a reaction with a known analyzing power A_p:

$$P_B = \frac{1}{A_p}\frac{N_L - N_R}{N_L + N_R}. \tag{14}$$

P_B is the beam polarization, N_L and N_R are the number of scatters left and right normalized by luminosity. A_p can be known from experiment or theory.

A physics asymmetry is the raw (measured) asymmetry, normalized by the beam polarization. Examples are

$$A_L = \frac{1}{P_B}\frac{N_+ - N_-}{N_+ + N_-} \tag{15}$$

$$A_{LL} = \frac{1}{P_B^2}\frac{N_{++} - N_{+-}}{N_{++} + N_{+-}}. \tag{16}$$

A_L and A_{LL} are single and double spin longitudinal asymmetries. N_+ and N_{+-} are the number of scatters observed with the beam polarization helicity + (one beam + and the other beam− for N_{+-}) normalized by luminosity. The beam polarization P_B is taken as the same for both beams for A_{LL}. For those reactions with a high degree of statistical accuracy, the error in the physics asymmetry is

$$\left(\frac{\delta A_L}{A_L}\right)^2 \sim \left(\frac{\delta P_B}{P_B}\right)^2 \tag{17}$$

$$\left(\frac{\delta A_{LL}}{A_{LL}}\right)^2 \sim 2\left(\frac{\delta P_B}{P_B}\right)^2. \quad (18)$$

Thus, if the absolute beam polarization is known to 10%, for example, then the single spin asymmetry A_L is uncertain to 10% of itself. Similarly, for A_{LL} the error becomes 20%. The beam polarization error only becomes significant when the statistical precision reaches the same level, thus a 10σ or 5σ measurement, respectively. We only anticipate a 10σ measurement for the u quark polarization in a polarized proton using parity violation of W^+ production, where the expected asymmetry A_L is quite large and, thus, the expected statistical contribution to $\delta A_L/A_L$ is small. Gluon polarization will be measured by direct photon production and the statistical contribution to $\delta A_{LL}/A_{LL}$ would approach 5σ only for maximal gluon polarization.

6.2. $p + C$ elastic scattering in CNI region

Small angle elastic scattering of hadrons in the Coulomb-Nuclear Interference (CNI) region has long been advocated for polarimetry. The predicted asymmetry is significant and largely independent of energy above a few GeV. The prediction rests on hadronic spin flip being small, which is expected for high energies. The CNI process has been proposed for RHIC polarimetry using a hydrogen jet target and in collider mode using the *pp2pp* experiment [38]. Both would be *pp* CNI. It is also possible to use a carbon target, *pC* CNI, which is simpler and cheaper than a hydrogen jet, and can be installed in the individual rings. In addition, the carbon target is easier to handle in the vacuum. The analyzing power for *pC* CNI is similar to *pp* CNI (both about 0.04), and the cross section is high, giving a very large figure of merit NA^2. However, for *pC* CNI at high energy with typical values of $-t$ from 0.002 to 0.01 GeV^2, scattering results in both a very small forward angle of the scattered proton and a very low kinetic energy of the Carbon recoil (0.1–1 MeV). It is impossible to measure the forward scattered proton without drastically reducing the beam divergence at the target which would severely reduce the scattering rate and also cause unacceptable beam emittance growth. It will therefore be necessary to rely only on the measurement of the recoil Carbon nuclei to identify elastic scattering. The low energy carbon nuclei would stop in most targets. The very thin ribbon carbon targets developed at IUCF [39] are crucial to the *pC* CNI polarimeter: both for survival in the RHIC beam and to get the carbon nuclei out of the target in the CNI region where the recoil carbon carries only hundreds of keV kinetic energy. The slowness of the recoil carbon makes detection difficult; however, the detector may be placed so that the arrival time of the carbon occurs before the passage of the next bunch, thus avoiding any prompt background.

Elastic scattering in the small angle CNI region is predicted to have a calculable analyzing power of about 3–5% as well as a large cross section over the whole RHIC energy range from 24 GeV/c to 250 GeV/c [40]. The analyzing power is given by

$$A_N(t) = \frac{Gt_0\sqrt{t}}{m_p(t^2 + t_0^2)} \quad (19)$$

where G is the anomalous magnetic moment of the proton (1.7928), m_p the proton mass, and $t_0 = 8\pi\alpha Z/\sigma_{tot}$. The total cross-section σ_{tot} is only weakly energy dependent over the relevant energy range. Fig. 16 shows the calculated analyzing power for a hydrogen target ($Z = 1$, $\sigma_{tot} = 35$ mb) and a carbon target ($Z = 6$, $\sigma_{tot} = 330$ mb [41]) as a function of $(-t)$. The uncertainty from a hadronic spin flip amplitude has been estimated to be smaller than 10% of the analyzing power from CNI. Using a carbon target will result in the high luminosity required for fast polarization measurements. The sizable analyzing power, the large cross section and the advantages of a solid ribbon target makes this process ideal for a fast primary polarimeter for RHIC.

6.3. Overall design

For easy maintenance, this has to be a warm straight section. The warm straight section between Q3 and Q4 at section 12 is assigned for both polarimeters in Blue and Yellow rings (see Fig. 7). Both target chambers are located near Q4 where the vertical and horizontal β functions are small

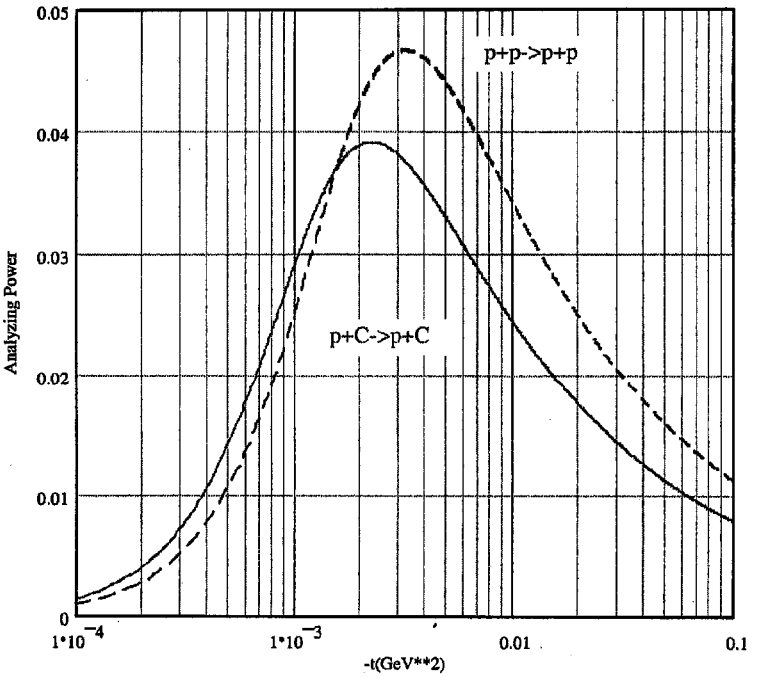

Fig. 16. Coulomb-Nuclear interference analyzing power for pp and pC scattering.

thus reducing the effect of multiple scattering on emittance dilution. Both target chambers are upstream of each other for their respective beam. Since beams are in opposite directions in the two rings, the detectors for both polarimeters are not in the scattering showers of each other.

It is desirable for the polarimeter to measure both horizontal and vertical beam polarization profiles. This requires separate targets scanning both vertically and horizontally. The current design of target holder is capable of holding 4 targets. Two stepping motors are used for each target assembly to drive a linear motion to move the whole assembly in and a rotary motion to pivot the desired target into the beam. An interlock relay system is in place to assure that at any time only one of the two assemblies can move a target into the beam.

In manipulating polarization in RHIC, information on both vertical and horizontal components of beam polarization are needed. In addition to one pair of detectors sitting in the horizontal plane, two pairs of detectors sitting at $\pm 45°$ are added, which are capable of measuring both transverse components (see Fig. 17). When using these two pairs for either vertical or radial components, the analyzing power will drop by a factor of $\cos 45° = \sqrt{2}/2$. At full RHIC designed intensity, the bunch width is about 2 ns and bunch spacing is 106 ns. To avoid the prompt

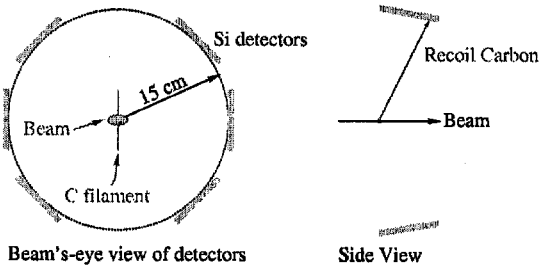

Fig. 17. Cross-section of the target chamber. Beam is going into the paper and hits the carbon target in the center of the beam pipe. The carbon target is 5.5 $\mu g/cm^2$ thick and 11.6 μm wide.

background, the carbon nuclei should arrive at the detectors between two bunches, i.e., within 100 ns. The Si detector can detect a carbon ion with kinetic energy as low as 100 keV, which can travel about 15 cm in 100 ns. The distance between detectors and interaction point is set as 15 cm.

The minimum target box length is determined by the relative positions of target, view port and detector sockets, which is 50.8 cm. To minimize the contribution to beam impedance [42], a 5:1 conical transition section is attached at each end of the vacuum chamber so that the total length of the chamber is 1.6 m.

6.4. *Event rates and emittance blowup*

In the CNI interference region, the cross sections of elastic and inelastic scattering are comparable. One can use the elastic cross section to estimate the event rates. Each Si detector has twelve 0.1 cm × 1 cm strips. The detectors are identical to those used in the AGS E950 experiment, and the strips were designed to obtain angle information. From the experience of E950, the angle information was not essential, so the strips are mounted parallel to the beam direction in RHIC. The event rate of each strip will only be one twelfth of the rate of the total detector.

The luminosity is given by

$$L = f_r N_p \frac{d_w d_t}{\sqrt{2\pi}\sigma_y}\left[\frac{\rho N_A}{A_w}\right] \tag{20}$$

where d_t and d_w are the thickness and width of the carbon ribbon, respectively, $A_w = 12$ gm/mol is the atomic weight of carbon and $N_A = 6.022 \times 10^{23}$ atoms/mol is Avogadro's number. This gives an event rate per bunch crossing of

$$R_{C,\text{crossing}} = L \cdot \delta\sigma = \frac{d_w d_t}{\sqrt{2\pi}\sigma_y}\left[\frac{\rho N_A}{A_w}\right]\delta\sigma \tag{21}$$

where $\delta\sigma$ is the cross-section. As the target is sitting in the beam, the emittance of the beam is increased due to multiple scattering. A total of 10^7 Carbons in the polarimeter is needed to obtain a 5% statistic error in polarization. It is useful to parameterize the resulting total emittance growth in terms of the total recoil Carbon events N_C:

$$\Delta\varepsilon_{(x,y)\text{tot}} = \frac{3\beta_{(x,y)}}{\beta^3\gamma}\frac{1}{L_{\text{rad}}}\left[\frac{0.0141}{0.938}\right]^2 \times \frac{N_C}{N_p}\left[\frac{A_w}{\rho N_A}\right]\frac{1}{\delta\sigma}[\pi] \tag{22}$$

where $\beta_{(x,y)}$ is the (x, y) lattice beta function at the target location, β and γ are the usual relativistic factors and $L_{\text{rad}} = 18.8$ cm is the radiation length of the target material.

Table 5
Rates estimates and emittance blowup for full luminosity. The following parameters were assumed: $\varepsilon_N = 10\pi$ μm, protons/fill = 120 bunches at 2×10^{11} protons/bunch

Detector set	Energy [GeV]	Time [s]	Δε [π μm]	Event rate per bunch
2 detectors	25	3.85	0.02	0.277
	250	1.22	0.002	0.554
4 detectors	25	2.72	0.014	0.391
	250	0.86	0.0014	1.238

With the relations given above, the event rates and measuring times are estimated as shown in Table 5. A carbon ribbon target of 4 μg/cm^2 was assumed. The emittance increase at 250 GeV/c is negligible, and such measurements could be made periodically throughout a fill. As can be seen from the table, measurement times are quite reasonable.

References

[1] I. Alekseev, et al., Design Manual Polarized Proton Collider at RHIC, Brookhaven National Laboratory, 1998.

[2] L.H. Thomas, Philos. Mag. 3 (1927) 1;
V. Bargmann, L. Michel, V.L. Telegdi, Phys. Rev. Lett. 2 (1959) 435.

[3] M. Froissart, R. Stora, Nucl. Instr. Meth. 1 (1960) 297.

[4] T. Khoe, et al., Part. Accel. 6 (1975) 213;
J.L. Laclare, et al., J. Phys. (Paris), Colloq. 46 (1985) C2-499;
H. Sato, et al., Nucl. Instr. Meth., Phys. Res. Sec. A 272 (1988) 617;
F.Z. Khiari, et al., Phys. Rev. D 39 (1989) 45.

[5] Ya.S. Derbenev, et al., Part. Accel. 8 (1978) 115.

[6] T. Roser, in: K.J. Heller (Ed.), AIP Conference Proceedings, Vol. 187, AIP, New York, 1988, p. 1442.
[7] M. Anerella, et al., Nucl. Instr. Meth. A 499 (2003) 280.
[8] W.W. MacKay, et al., Superconducting Helical Snake Magnets: Design and Construction, DESY-PROC-1999-03, p. 163.
[9] J.G. Alessi, et al., AIP Conf. Proc. 187 (1988) 1221.
[10] A.N. Zelenski et al., Optically-pumped polarized H^- ion sources for RHIC and HERA colliders, Proceedings of PAC 1999, 1999, p. 106.
[11] F.Z. Khiari, et al., Phys. Rev. D 39 (1989) 45.
[12] T. Roser, AIP Conf. Proc. 187 (1988) 1442.
[13] H. Huang, et al., Phys. Rev. Lett. 73 (1994) 2982.
[14] M. Bai, et al., Phys. Rev. Lett. 80 (1998) 4673.
[15] T. Roser, Proceedings of the 10th International Symposium on High Energy Spin Physics, Nagoya, Vol. 429, 1992.
[16] T. Roser, M. Syphers, E. Courant, L. Ratner, M. Okamura, Helical partial snake for the AGS, BNL Internal Report AGS/RHIC/SN-072, March, 1998.
[17] S.Y. Lee, E.D. Courant, BNL Technical Note AD/RHIC-63.
[18] J. Claus, H. Foelsche, Beam transfer from AGS to RHIC, RHIC 47, 1988.
[19] N. Tsoupas, E. Rodger, J. Claus, H.W. Foelsche, P. Wanderer, BNL Design and B-field measurements of a Lambertson injection magnet for the RHIC machine, Proceedings of PAC 1995, Vol. 2, 1995, p. 1352.
[20] V.I. Ptitsin, Yu.M. Shatunov, Helical spin rotators and snakes, in: A. Luccio, Th. Roser (Eds.), Proceedings of the Third Workshop on Siberian Snakes and Spin Rotators, Upton, NY, Sept. 12–13, 1994, Brookhaven National Laboratory Report BNL-52453, p. 15.
[21] A.U. Luccio, Program SNIG, unpublished, and SNIG Formalism Proc. Third Workshop on Siberian Snakes, loc. cit., p. 193. Also: "Numerical Optimization of Siberian Snakes and Spin Rotators for RHIC", Proceedings Adriatico Conf. Trieste, Italy, Dec. 1995, World Scientific, Singapore; Spin Note AGS/RHIC/SN008.
[22] A.U. Luccio, Optimization of spin angles from a helix field map, Spin Note AGS/RHIC/SN042, Upton, Nov. 5, 1996.
[23] E. Courant, Orbit matrices for helical snakes, BNL Internal Report RHIC/AP/47, November, 1994.
[24] F. Pilat, Linear coupling effect of the helical snakes and rotators in RHIC, BNL Internal Report RHIC/AP/56, February, 1995.
[25] M.J. Syphers, Closed orbit errors from helical dipole magnets, BNL Internal Report AGS/RHIC/SN-016, January, 1996.
[26] M.J. Syphers, Total pitch specification for RHIC helical dipole magnets, BNL Internal Report AGS/RHIC/SN-058, August, 1997.
[27] M. Okamura, Optimization of rotation angle of the helical dipole magnets, BNL Internal Report AGS/RHIC/SN-061, August, 1997.
[28] A.K. Jain, Estimation of rotation angle in the full length helical dipole based on data in the half-length prototype HRC001, BNL Internal Report AGS/RHIC/SN-062, September, 1997.
[29] M.J. Syphers, Field quality issues for RHIC helical dipole magnets, BNL Internal Report AGS/RHIC/SN-015, January, 1996.
[30] T. Katayama, Multipole field expansion of helical magnet, BNL Internal Report AGS/RHIC/SN-038, September, 1996.
[31] W. Fischer, Preliminary tracking results with helical magnets in RHIC, BNL Internal Report AGS/RHIC/SN-034, August, 1996.
[32] B. Autin, Y. Marti, Closed orbit correction of alternating gradient machines using a small number of magnets, CERN/ISR-MA/73-17, CERN, 1973.
[33] J. Wei, Magnet quality and collider performance prediction, BNL Internal Report RHIC/AP/117, November, 1996.
[34] S.Y. Lee, S. Tepikian, Phys. Rev. Lett. 56 (1986) 1635.
[35] T. Roser, Spin rotators and split siberian snakes, Nucl. Instr. Meth. A 342 (1994) 343.
[36] R.A. Phelps, Spin flipping a stored polarized proton beam in the presence of Siberian Snakes, Third Workshop on Siberian Snakes, loc. cit., p. 225.
[37] M. Bai, et al., Phys. Rev. E 56 (1997) 6002.
[38] W. Guryn, Proceedings of Workshop on Jet Targets at RHIC, January, 2000.
[39] W.R. Lozowski, J.D. Hudson, Nucl. Instr. Meth. A 334 (1993) 173.
[40] N.H. Buttimore, et al., Phys. Rev. D 18 (1978) 694;
N.H. Buttimore, AIP Conference Proceedings, Vol. 95, AIP, New York, 1983, p. 634.
[41] J.L. Rosen, AIP Conference Proceedings, Vol. 26, AIP, New York, 1975, p. 287.
[42] H. Wang, H. Huang, RHIC Polarimeter Impedance Analysis with MAFIA, RHIC/AP/178 (October, 1999).